






Title	Prediction models for the flux decay profile and initial flux of microfiltration for therapeutic proteins
Author(s)	Inoue, Kota; Masuda, Yumiko; Torisu, Tetsuo et al.
Citation	Biotechnology and Bioengineering. 2024, 121(6), p. 1889-1901
Version Type	VoR
URL	https://hdl.handle.net/11094/95748
rights	This article is licensed under a Creative Commons Attribution 4.0 International License.
Note	

Osaka University Knowledge Archive : OUKA

<https://ir.library.osaka-u.ac.jp/>

Osaka University

Prediction models for the flux decay profile and initial flux of microfiltration for therapeutic proteins

Kota Inoue^{1,2}  | Yumiko Masuda¹  | Tetsuo Torisu²  | Koichi Nonaka¹  |
Susumu Uchiyama² 

¹Biotechnology Research Laboratories, Biologics Division, Daiichi Sankyo Co., Ltd, Chiyoda-machi, Japan

²Department of Biotechnology, Graduate School of Engineering, Osaka University, Suita, Japan

Correspondence

Susumu Uchiyama, Department of Biotechnology, Graduate School of Engineering, Osaka University, 2-1 Yamadaoka, Suita, Osaka, 565-0871, Japan.
Email: suchi@bio.eng.osaka-u.ac.jp

Present addresses

Kota Inoue, Modality Research Laboratories, Research Function, R&D Division, Daiichi Sankyo Co., Ltd, Shinagawa-ku, Japan.

Yumiko Masuda, Production Department I, Onahama Plant, Daiichi Sankyo Chemical Pharma Co., Ltd, Iwaki, Japan.

Koichi Nonaka, Biologics Division, Technology Supervisory Division, Daiichi Sankyo Co., Ltd, Chiyoda-machi, Japan.

Funding information

Japan Agency for Medical Research and Development (AMED), Grant/Award Numbers: 22ae0121013h0602, 22ak0101188j0001

Abstract

Microfiltration (MF) is an essential step during biopharmaceutical manufacturing. However, unexpected flux decay can occur. Although the flux decay profile and initial flux are important factors determining MF filterability, predicting them accurately is challenging, as the root cause of unexpected flux decay remains elusive. In this study, the methodology for developing a prediction model of flux decay profiles was established. First, the filtration profiles of different monodisperse polystyrene latex and silica beads of various sizes were evaluated. These results revealed that the size and surface electrostatic properties of the beads affect the flux decay profile. Taking the size and surface electrostatic properties of protein aggregates into account, we constructed a predictive model using model bead filtration profiles. We showed that this methodology was applicable to two different MF filters to predict the flux decay profile of therapeutic proteins. Because our proposed prediction model is based on normalized flux, the initial flux is required to predict the overall filtration profile. Then, we applied the Hagen–Poiseuille equation using sample viscosity values to estimate the initial flux. The developed prediction models can be used for effective MF scale-up assessment during the early stages of process development.

KEYWORDS

filter fouling, flux decay, initial flux, microfiltration, prediction model, protein aggregates

1 | INTRODUCTION

Microfiltration (MF) is crucial for biopharmaceutical manufacturing to reduce the risk of microbial contamination and avoid adverse effects on patients. MF are typically conducted after multiple steps during one manufacturing batch (Minow et al., 2012). A nominal 0.22 μ m-rated MF can effectively remove all microorganisms except viruses

and mycoplasma (Nikfarjam & Farzaneh, 2012; Robertson et al., 1998). However, unexpected filter fouling can delay manufacturing or increase the risk of microbial contamination. Nevertheless, the root cause of unexpected flux decay remains unknown.

Generally, the V_{\max} (maximum filtrate volume per unit area) methodology is commonly used to screen filter types and to estimate the minimum filter area required for large-scale manufacturing. In this

This is an open access article under the terms of the [Creative Commons Attribution](https://creativecommons.org/licenses/by/4.0/) License, which permits use, distribution and reproduction in any medium, provided the original work is properly cited.

© 2024 The Authors. *Biotechnology and Bioengineering* published by Wiley Periodicals LLC.

method, samples with similar properties derived from large-scale manufacturing is required to filter at constant pressure using a small lab-scale MF filter. The V_{\max} can then be extrapolated from a flux decay profile via a standard blocking mechanism (Joseph et al., 2016; Zydney & Ho, 2002). Nevertheless, some unresolved issues remain. For example, ~100 mL of sample is typically required for a single lab-scale filtration experiment, making it difficult to conduct trials during the early stages of process development. Thus, identifying the cause of unexpected flux decay remains challenging. Moreover, the quality of a biopharmaceutical sample depends on the manufacturing setup, including mixing equipment, which influences the degree of protein aggregates that are generated via a "mixing mechanism" (Ishikawa et al., 2010; Sediq et al., 2016; Gikanga et al., 2015, 2017, 2020) and by pumps (Nayak et al., 2011; Her & Carpenter, 2020; Wu & Randolph, 2020). Thus, the quality of samples greatly varies between lab- and large-scale manufacturing, especially regarding the size distribution of protein aggregates generated before the MF. Although several reports showed that MF filterability and the amount of micron-sized particles, typically representing protein aggregates, are negatively correlated (Ishikawa et al., 2010; Callahan et al., 2014; Gikanga et al., 2015), the quantitative relationship between filterability and particle characteristics (i.e., size and amount) remains unclear.

In this study, we evaluated the correlation between the size of foulants and MF filter fouling then developed a prediction model for flux decay profiles based on quantitative information of the size distribution of protein aggregates. Moreover, we also demonstrated that the initial flux of MF follows the Hagen–Poiseuille equation such that the initial flux can be predicted from the sample viscosity.

2 | MATERIALS AND METHODS

2.1 | Materials

Eight monoclonal antibodies (mAb1–8) and a Fc-fusion protein (Fc-fusion1) were expressed in Chinese hamster ovary cells and highly purified via multiple chromatography steps. National Institute of Standards and Technology Traceable Particle Size Standards, made up of polystyrene latex (PSL) with diameters of 40, 100, 200, and 500 nm as well as 1, 2, and 4 μm , and 200 nm surface modified PSL beads with amino (NH_2) groups were purchased from Polysciences, Inc. Surface unmodified silica beads and surface modified silica beads with amino (NH_2) groups (with diameters of 200 and 500 nm, as well as 1, 1.5, and 4 μm for both silica beads) were purchased from micromod Partikeltechnologie GmbH.

2.2 | Lab-scale ultrafiltration/diafiltration (UF/DF) samples for side-by-side filtration experiments

To conduct MF experiments in parallel, six highly purified mAbs (mAb1–6) were processed by protein A affinity chromatography and eluted with 120 mM acetate buffer (pH 3.6) for buffer exchange. The

pH of the eluates was then adjusted to 5 with 1 M Tris and diluted twofold with 50 mM acetate buffer (pH 5.0). The sample concentration was ranged in 13–14 mg/mL after dilution. Next, DF were conducted against 10 mM histidine with 5% sorbitol (pH 5.5) with lab-scale UF/DF system. After the DF step, each mAb was concentrated to 50 mg/mL.

2.3 | Preparation of protein aggregate-enriched samples for filtration experiments and zeta potential measurements

Protein aggregates were enriched by either contact agitation or orbital shaking stress. Details of experimental conditions for contact agitation and orbital shaking stress are in the supplementary material. Protein aggregate-enriched samples by either contact agitation or orbital shaking were used for filtration experiments. Next, to measure the zeta potentials of the protein aggregates, 2 mg/mL of mAb2 that underwent 24 h contact agitation or orbital shaking stress were centrifuged at 15,000g at 20°C for 60 min. The supernatants and resuspended pellets were measured the zeta potential and protein aggregation profile.

2.4 | Filtration experiments

Filtration experiments were conducted using 0.5/0.2 μm polyether-sulfone (PES) bilayer filters (Filter A) and 0.22 μm polyvinylidene difluoride filters (Filter B) supplied by Merck KGaA. Each experiment was conducted using a 3.5 cm^2 filter at 0.1 MPa constant pressure under room temperature. The total weight of filtrate was recorded by the balance every 10 s and the recorded weight was converted to the volume with the assumption for the density of 1.0 g/cm^3 . The initial flux, J_0 , was determined as the maximum flux observed during the initial filtration stages. V_{\max} was then calculated using the following equation (Zydney & Ho, 2002; Joseph et al., 2016).

$$\frac{t}{V} = \frac{1}{Q_0} + \left(\frac{1}{V_{\max}} \right) t. \quad (1)$$

Here, V is the total filtrate volume per unit area, t represents time, and Q_0 is the initial flux. For filtration experiments, each PSL and silica bead was suspended at 100 $\mu\text{g}/\text{mL}$ in three buffers: (a) 10 mM histidine with 5% sorbitol (pH 5.5); (b) 120 mM acetate buffer (pH 5.0); and (c) 50 mM acetate buffer (pH 5.0) with 0.2 M NaCl. To analyze the fouling model, filtration results were fitted to one of five types of filter fouling model. K_s , K_b , K_i , K_c , and K_a represent the constants of each fouling model (Bolton et al., 2006).

$$\text{Standard blocking: } \frac{J}{J_0} = \left(1 - \frac{K_s V}{J_0} \right)^2, \quad (2)$$

$$\text{Complete blocking: } \frac{J}{J_0} = 1 - \frac{K_b V}{J_0}, \quad (3)$$

$$\text{Intermediate blocking: } \frac{J}{J_0} = e^{-K_f V}, \quad (4)$$

$$\text{Cake filtration: } \frac{J}{J_0} = \frac{1}{K_c J_0 V + 1}, \quad (5)$$

$$\text{Adsorption: } \frac{J}{J_0} = \left(1 - \frac{5K_a V}{J_0}\right)^{4/5}. \quad (6)$$

Model fitting as per the Gauss–Newton method was conducted using JMP® version 14.0.0 (SAS Institute Inc.). The best fit model for each filtration result was determined by comparing root mean squared error (RMSE) values. For the initial flux prediction, trehalose dihydrate (Wako Special Grade, FUJIFILM Wako Pure Chemical Corporation) was dissolved in water at 10, 20, 30, and 40 w/w%.

2.5 | Quantitative laser diffraction (qLD)

Submicron- to micron-sized particles were evaluated using the qLD method (Totoki et al., 2015; Yoneda et al., 2019) by the Aggregates Sizer (Shimadzu Corporation). The values of the refractive index and density were 1.46 and 1.37 g/cm³ for proteins (software intrinsic). The noise cutoff level was set to 100. Further information is in the Supporting Information.

2.6 | Size-exclusion high-performance liquid chromatography (SE-HPLC)

Monomer loss values (%) for mAbs were evaluated by SE-HPLC using a TSKgel UltraSW Aggregate column (7.8 mm I.D. × 300 mm) (Tosoh Corporation). The column oven was maintained at 25°C. Using 0.1 M sodium phosphate buffer (pH 7.0) with 0.4 M NaCl as the mobile phase, isocratic measurements were taken at a flow rate of 0.5 mL/min. Proteins were detected at a wavelength of 280 nm.

2.7 | Zeta potential and viscosity measurements

The zeta potential was measured by laser Doppler electrophoresis (Tucker et al., 2015) using a Zetasizer Nano ZSP instrument (Malvern Panalytical).

Viscosity was measured at 20°C by a microfluidic shear viscometer (Solomon et al., 2016) using Honeybun (Unchained Labs).

3 | RESULTS AND DISCUSSION

3.1 | Side-by-side filtration experiments using six mAbs

Six highly purified mAbs (mAb1–6), processed by protein A affinity chromatography and lab-scale UF/DF, were filtered using either

Filter A or B. Figure 1 shows the size distribution of these proteins pre- and post-UF/DF, and after filtration with Filters A or B as measured by qLD. The peak around 100 nm existed in initial samples for all mAbs. Particles around 200 nm to several tens of micrometers were increased by UF/DF processing, whereas the size distribution varies among mAbs 1–6. For mAb1, the amount of particles below 1 μm were relatively small, whereas the distribution gradually increased between 1 and 50 μm at low level. For mAbs 2 and 3, the particles gradually increased from around 1 to 100 μm. Meanwhile, as for mAbs 4–6, the particles increased from 200 nm to several tens of microns, with a significant amount in the range of several micrometers. Most of these protein aggregates were removed by MF using filter A or filter B, except for those with particle sizes <200 nm.

The rank order of filterability of the mAbs based on V_{\max} in descending order studied here was as follows: mAb1, mAb2, mAb3, mAb4, mAb5, and mAb6 for Filter A (Supporting Information S1: Figure S1a), and mAb2, mAb3, mAb1, mAb4, mAb5, and mAb6 for Filter B (Supporting Information S1: Figure S1b). These results indicate a difference in filterability between Filters A and B for these six mAbs. Previous studies have shown that the amount of micron-sized protein aggregates was negatively correlated with the filterability of MF filters (Ishikawa et al., 2010; Callahan et al., 2014; Gikanga et al., 2015). Although the total concentration of particles sized 200 nm to 2 μm was negatively correlated with V_{\max} (Supporting Information S1: Figure S2), the data obtained here was insufficient to precisely predict filterability. Therefore, in addition to the concentration, the size distribution of protein aggregates within a specific size range (i.e., 200 nm to a few micrometers) is important for predicting the filter fouling behavior.

3.2 | Filtration experiments with model beads

To evaluate the correlation between the amount of protein aggregates loaded onto the filter and filter fouling profiles, mAb samples containing monodisperse protein aggregates within a specific size range are ideal. Nevertheless, generating these mAb samples stably and repeatedly is difficult. Therefore, we used PSL (i.e., 40, 100, 200, and 500 nm, as well as 1, 2, and 4 μm) and silica beads (i.e., 200 and 500 nm, as well as 1, 1.5, and 4 μm) to evaluate flux decay profiles. Each bead was suspended in three different buffers and the dispersity for each combination of bead and buffer was evaluated using dynamic light scattering (Supporting Information S1: Figure S3). Filtration experiments conducted with filter A showed that beads with a diameter ≥4 μm did not cause filter fouling (Figure 2). However, beads with diameters ranging from 500 nm to 2 μm caused filter fouling, and the flux decay profile depended on particle size. Importantly, for beads within this size range, neither the material and surface modification of the beads nor the composition of the buffer used for suspending the beads significantly influenced flux decay profiles. In contrast, the filtration profiles of suspended beads with diameters ≤200 nm were affected by bead material and

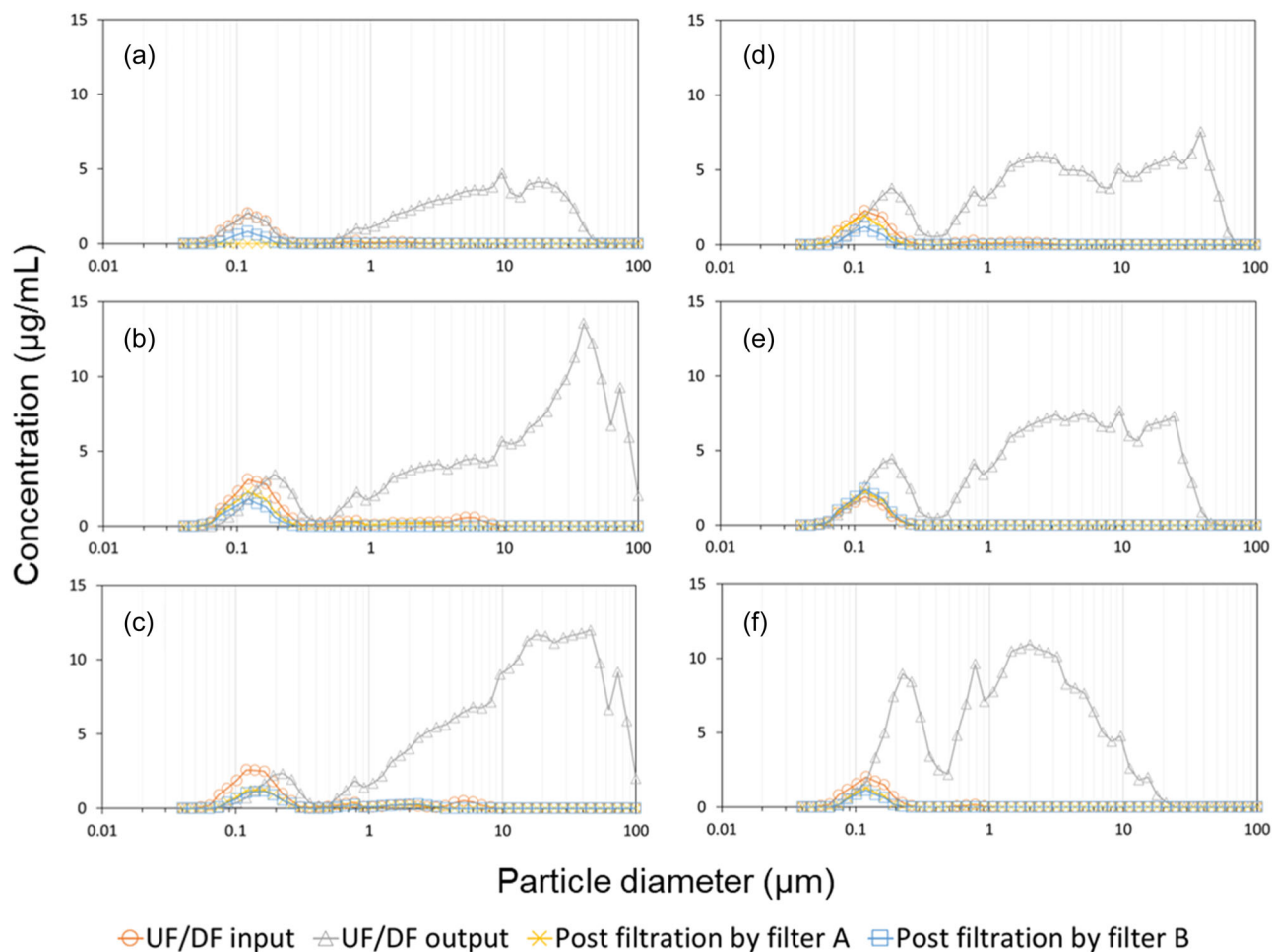


FIGURE 1 Quantitative analysis of submicron- and micron-sized particles for six monoclonal antibodies. Samples: (a–f) mAb1–6.

buffer composition. Moreover, the flux decay profiles of beads ≤ 200 nm in diameter—including ones of the same diameter—were affected by some (but not all) combinations of bead materials and buffers.

Next, the model beads filtration results were fitted to filter fouling models (Supporting Information S1: Figure S4). For beads ranging from 500 nm to 2 μm , the cake filtration model was the best fit, as it assumes particle deposition on the filter surface. Therefore, the size-exclusion mechanism was dominant for these beads, which were larger than the pore size of Filter A. For beads ≤ 200 nm, filter fouling models, such as the adsorption, standard blocking, or internal blocking models showed the best fit. Furthermore, as Filter A has a bilayer structure in which the pore sizes of the upper and lower layers are 500 and 200 nm, respectively, beads ≤ 200 nm can pass through the upper layer of the filter, but can foul the second filter layer. Importantly, buffer components, total protein concentrations, and the solution viscosity have no impact on flux decay profiles (Supporting Information S1: Figures S5 and S6). We considered that filter fouling could be caused by particles of a specific size, with dependent on the loading amount of those particles.

3.3 | Surface electrostatic properties of model beads and protein aggregates

As mentioned previously, the bead material and buffer composition are important factors determining filter fouling. Trinh et al. (2020) reported that foulant surface charges determine the internal fouling of MF. In addition, Han et al. (2018) reported that the surface charge of monodisperse particulate foulants affected pore blockage and cake morphology at the membrane surface. Based on this information, understanding the surface electrostatic properties of model beads and protein aggregates is important for developing a prediction model for the filter fouling profiles of protein samples based on filtration profiles for model beads. First, the zeta potentials of model beads were measured for each bead-buffer combination (Table 1a). PSL and surface unmodified silica beads showed negative zeta potential, while silica beads with a diameter of 500 nm, 1, or 1.5 μm whose surface modified with an amino group showed positive zeta potential values. The amino group-modified silica or PSL beads with a diameter of 200 nm both had negative zeta potentials (Table 1a).

Next, the zeta potentials of submicron- to micron-sized protein aggregates were measured. As the samples obtained after UF/DF for

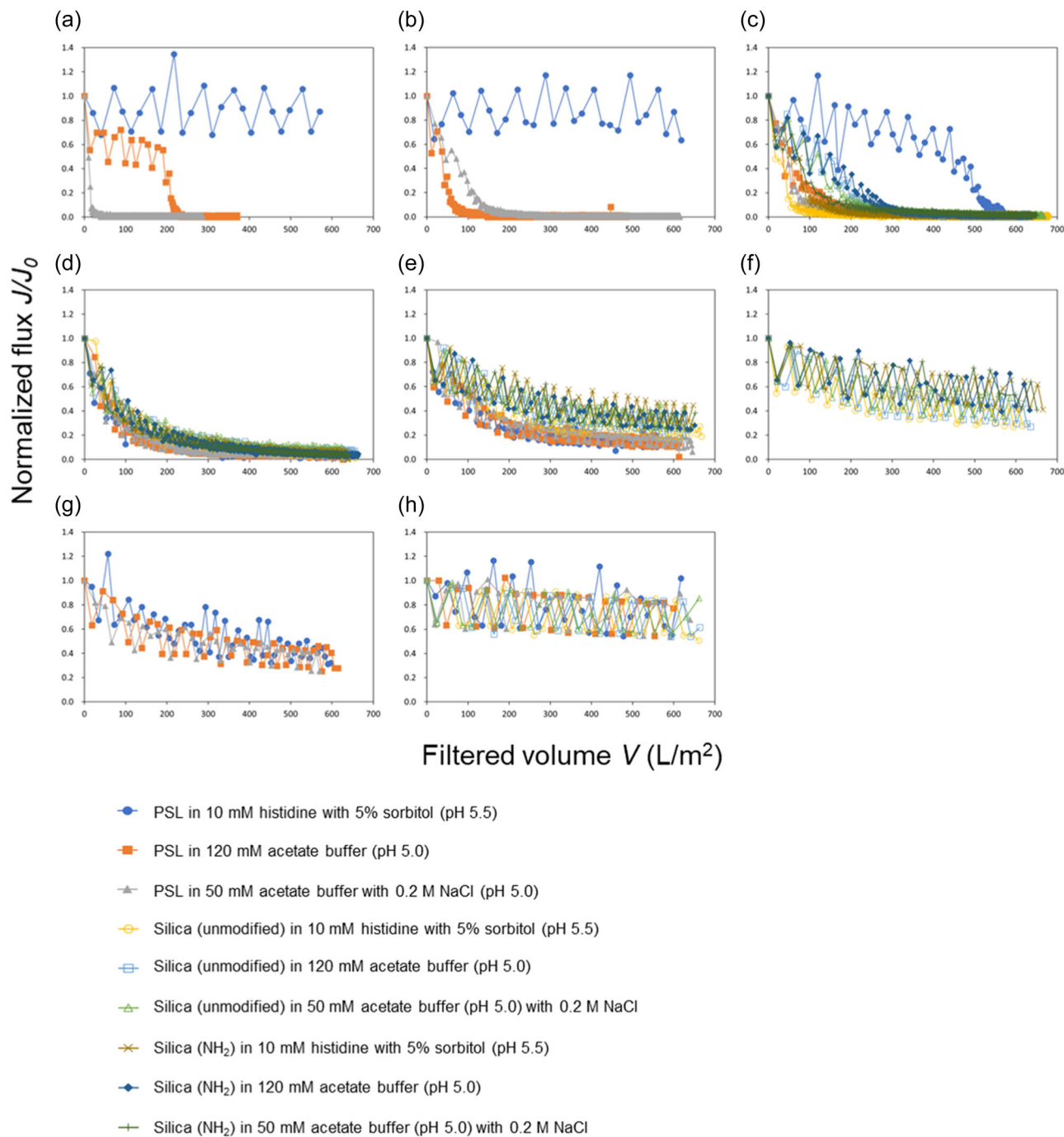


FIGURE 2 Filtration experiments for polystyrene (PSL) and silica size standard beads for Filter A. Diameters: (a) 40 nm, (b) 100 nm, (c) 200 nm, (d) 500 nm, (e) 1 μm , (f) 1.5 μm , (g) 2 μm , and (h) 4 μm .

side-by-side filtration experiments contained over 95% monomers, as evaluated by SE-HPLC, the submicron- to micron-sized protein aggregates needed to be enriched to determine their zeta potentials. As contact agitation with a magnetic stirrer is known to generate protein aggregates (Sediq et al., 2016; Gikanga et al., 2017), we took advantage of this to generate protein aggregates for the zeta potential measurement. Two types of interfacial stress conditions, that is, contact agitation and orbital shaking stress, were applied to mAb2 to enrich submicron- to micron-sized protein aggregates. SE-HPLC analysis showed that all

monomers were lost after 24 h contact agitation stress (Supporting Information S1: Table S1) and submicron- to micron-sized protein aggregates were generated (Supporting Information S1: Figure S7). In contrast, SE-HPLC also showed that mAb2 monomer remained after 24 h orbital shaking stress, but submicron- to micron-sized protein aggregates could subsequently be separated by centrifugation at 15,000g and 20°C for 60 min (Supporting Information S1: Table S1 and Figure S8). Comparing Supporting Information S1: Figures S7 and S8, the size of the protein aggregates generated by contact agitation stress was less than

TABLE 1 Zeta potential measurements for (a) polystyrene (PSL) and silica size standard beads, and (b) protein aggregates. Each zeta potential measurement was conducted in triplicate. The average and standard deviation (SD) were calculated, and are indicated as Average \pm SD.

	Zeta potential (mV)		120 mM acetate buffer (pH 5.0)		50 mM acetate buffer (pH 5.0) with 0.2 M NaCl	
	PSL (Unmodified) (NH ₂)	Silica (Unmodified) (NH ₂)	PSL (Unmodified) (NH ₂)	Silica (Unmodified) (NH ₂)	PSL (Unmodified) (NH ₂)	Silica (Unmodified) (NH ₂)
40 nm	-44.0 \pm 0.8		-33.9 \pm 0.7		-45.1 \pm 1.9	
100 nm	-49.6 \pm 1.1	Not tested	-27.4 \pm 0.9	Not tested	-10.6 \pm 0.7	Not tested
200 nm	-59.5 \pm 1.1	-37.7 \pm 0.4	-31.1 \pm 0.6	-31.5 \pm 0.8	-23.2 \pm 1.7	-11.2 \pm 0.3
500 nm	-76.1 \pm 2.3		-20.5 \pm 0.2	49.6 \pm 0.9	-40.2 \pm 1.7	-8.42 \pm 1.0
1 μ m	-84.2 \pm 1.4		-29.6 \pm 2.2	57.1 \pm 2.9	-43.3 \pm 0.1	-10.0 \pm 1.2
1.5 μ m	Not tested		-33.6 \pm 0.7	8.35 \pm 0.5	Not tested	-8.42 \pm 0.7
2 μ m	-76.0 \pm 1.0		-25.0 \pm 1.0		-22.6 \pm 0.6	
4 μ m	Not tested		-9.33 \pm 1.5		Not tested	
	Zeta potential (mV)		5,000g, 20°C, 60 min		15,000g, 20°C, 60 min	
	Initial	Contact agitation 24 h	Pellet	Sup.	Pellet	Sup.
10 mM histidine with 5% sorbitol (pH 5.5)	8.37 \pm 0.5	12.9 \pm 0.6	12.1 \pm 0.4	9.85 \pm 1.3	14.3 \pm 0.2	10.6 \pm 0.8
120 mM acetate buffer (pH 5.0)	4.49 \pm 0.7	6.82 \pm 0.1	5.30 \pm 0.4	4.00 \pm 0.9	5.98 \pm 0.6	5.26 \pm 0.8
50 mM acetate buffer (pH 5.0) with 0.2 M NaCl	2.92 \pm 1.3	3.72 \pm 0.2	0.972 \pm 1.7	2.03 \pm 1.1	3.64 \pm 0.4	2.19 \pm 0.7

TABLE 2 Summary of the best fit models for each particle size determined by fitting five different filter fouling models.

(a) Filter A				
Size	200 nm	500 nm	1 μm	2 μm
Beads, buffer	Silica (NH ₂), 120 mM acetate buffer (pH 5.0)	Silica (NH ₂), 120 mM acetate buffer (pH 5.0)	Silica (NH ₂), 120 mM acetate buffer (pH 5.0)	PSL, 120 mM acetate buffer (pH 5.0)
Best fit model	Intermediate blocking $\frac{J}{J_0} = e^{-K_i \frac{C_{200\text{nm}}}{100} \alpha V}$	Cake filtration $\frac{J}{J_0} = \frac{1}{K_c J_0 \frac{C_{500\text{nm}}}{100} V + 1}$	Cake filtration $\frac{J}{J_0} = \frac{1}{K_c J_0 \frac{C_{1\mu\text{m}}}{100} V + 1}$	Cake filtration $\frac{J}{J_0} = \frac{1}{K_c J_0 \frac{C_{2\mu\text{m}}}{100} V + 1}$
Parameters determined by filtration experiments	K_i : 0.0081862454 J_0 : 198.8571	K_c : 0.0001604638 J_0 : 195.4286	K_c : 0.0000291577 J_0 : 188.5714	K_c : 0.0000240577 J_0 : 173.1429
(b) Filter B				
Size	200 nm	500 nm	1 μm	2 μm
Beads, Buffer	Silica (NH ₂), 120 mM acetate buffer (pH 5.0)	Silica (NH ₂), 120 mM acetate buffer (pH 5.0)	Silica (NH ₂), 120 mM acetate buffer (pH 5.0)	PSL, 120 mM acetate buffer (pH 5.0)
Best fit model	Cake filtration $\frac{J}{J_0} = \frac{1}{K_c J_0 \frac{C_{200\text{nm}}}{100} \beta V + 1}$	Cake filtration $\frac{J}{J_0} = \frac{1}{K_c J_0 \frac{C_{500\text{nm}}}{100} \beta V + 1}$	Cake filtration $\frac{J}{J_0} = \frac{1}{K_c J_0 \frac{C_{1\mu\text{m}}}{100} \beta V + 1}$	Cake filtration $\frac{J}{J_0} = \frac{1}{K_c J_0 \frac{C_{2\mu\text{m}}}{100} \beta V + 1}$
Parameters determined by filtration experiments	K_c : 0.0003424725 J_0 : 70.2857	K_c : 0.0000798385 J_0 : 118.0952	K_c : 0.0000134023 J_0 : 108.0000	K_c : 0.0000171047 J_0 : 121.9048

Note: α and β are correction factors.

was obtained using orbital shaking stress. Table 1b indicated that enriched protein aggregates had a similar positive zeta potential as unstressed antibody monomers. Moreover, the isoelectric points (pIs) of six mAbs (mAb1–6) ranged between 6 and 9. Based on the correlation between the pI values of the six mAbs and the pHs of the buffers used, other mAbs were also expected to have positive zeta potential. As the material for Filter A was PES, the filter matrix might have negative zeta potential under three buffer conditions (Breite et al., 2019). Next, the surface electrostatic properties for model beads and protein aggregates will be considered in the next section to develop a prediction model for the flux decay profiles of protein samples.

3.4 | Flux decay profile prediction model

We hypothesize that an observed flux decay profile can break down to the flux decay of each particle size. The following equation (Equation 7) is proposed as the prediction model for the flux decay profile of MF.

$$\left(\frac{J}{J_0}\right)_{\text{predicted}} = \left(\frac{J}{J_0}\right)_{200\text{nm}} \times \left(\frac{J}{J_0}\right)_{500\text{nm}} \times \left(\frac{J}{J_0}\right)_{1\mu\text{m}} \times \left(\frac{J}{J_0}\right)_{2\mu\text{m}}. \quad (7)$$

Equation 7 characterizes the multiplication of a normalized flux, J/J_0 , for each particle size. The normalized flux for each particle size with a nondimensional parameter is employed to appropriately multiply the contribution of particles with different sizes. Due to the limitation of analytical methods, ≥ 200 nm particles were included in the equation. As described in Table 2a, in the case of Filter A, the best-fit model and

determined parameters for each model bead were included in the prediction formula to estimate the loading amount for each specific size of particle. To apply this formula to mAb solutions containing protein aggregates, 200 nm to 2 μm protein aggregates in mAb solutions were quantified using qLD. Model beads experiments were conducted using a concentration of each bead of 100 $\mu\text{g}/\text{mL}$; therefore, the volume, V , is corrected by the loading amount of particles. For 200 nm particles, filtration data for amino group-modified silica beads suspended in 120 mM acetate buffer (pH 5.0) was selected. As indicated in Table 1a, this bead contained an opposite sign zeta potential relative to protein aggregates. However, the absolute value of the zeta potential was smaller in this condition. Trinh et al. (2020) reported that colloidal foulants that had a smaller absolute value of the zeta potential caused considerable internal fouling when the membrane and colloidal foulants had the same sign zeta potential. For particle sizes of 500 nm and above, combining results in Figure 2 and Table 1a shows that particle surface electrostatic properties did not affect filter fouling relative to 200 nm beads. Thus, the combination of the bead and buffer, which show the same positive zeta potential same as the protein aggregates, were selected for 500 nm and 1 μm beads. As there was no product lineup for 2 μm silica beads, the filtration data for 2 μm surface unmodified PSL beads suspended in 120 mM acetate buffer (pH 5.0) was used.

First, filtration experiments of the mixture of different sizes of model beads were conducted using Filter A. Figure 3a shows a result for mixtures of beads that do not include 200 nm beads. This filtration profile was well predicted by Equation 7. Figure 3b,c show results for mixtures of beads containing 200 nm amino group-modified silica beads. These filtration profiles were also well predicted by Equation 7 (RMSE < 0.006)

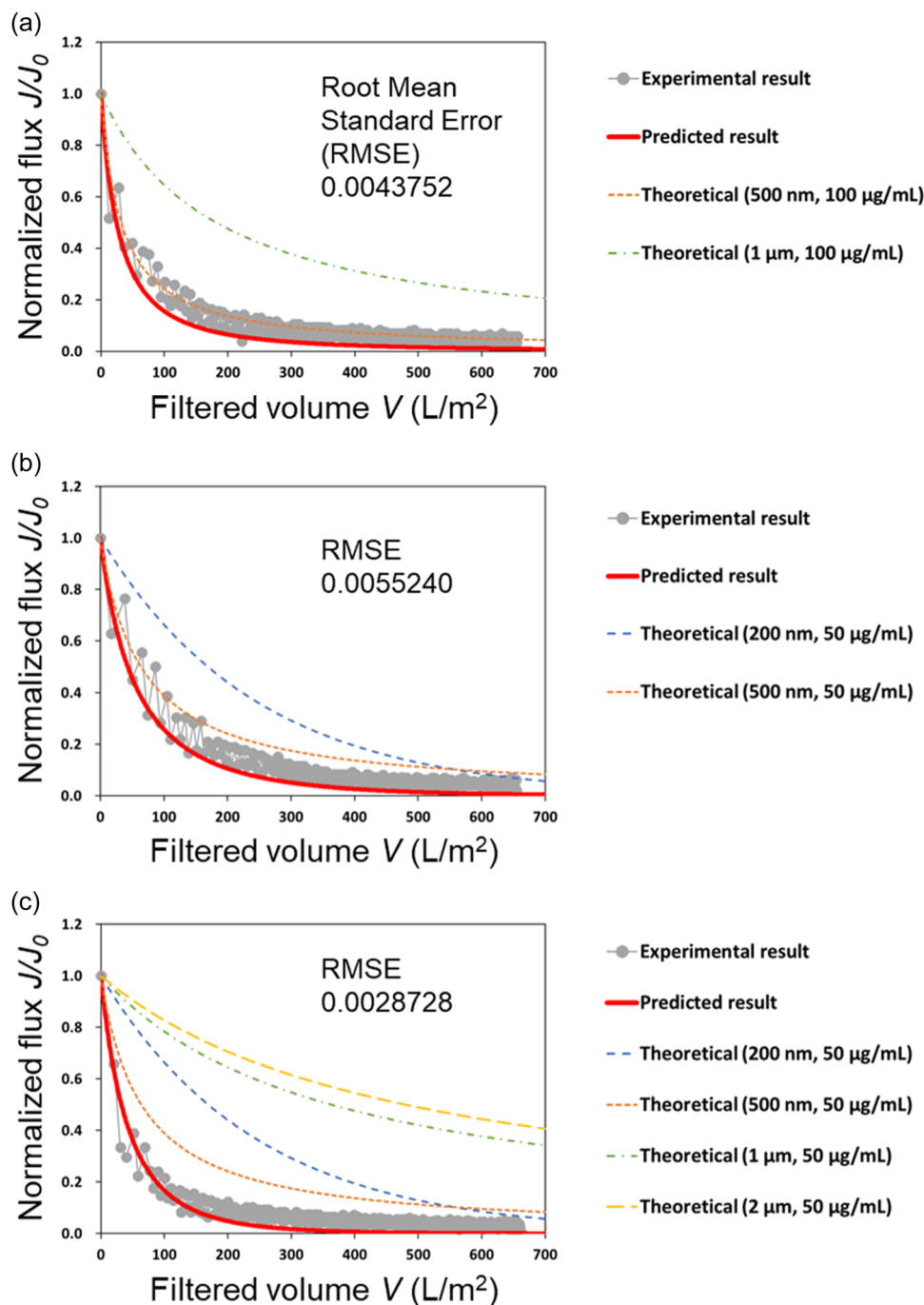


FIGURE 3 Predicted filtration profiles for different bead mixtures using Filter A. The samples contained a mixture of (a) 500 nm and 1 μm silica (NH_2) beads (both at 100 $\mu\text{g}/\text{mL}$); (b) 200 nm and 500 nm silica (NH_2) beads (both at 50 $\mu\text{g}/\text{mL}$); (c) 200 nm, 500 nm, and 1 μm silica (NH_2) beads with 2 μm PSL beads (all at 50 $\mu\text{g}/\text{mL}$). All mixtures were suspended in 120 mM acetate buffer (pH 5.0).

(Figure 3), as both mixtures were suspended in 120 mM acetate buffer (pH 5.0), which matched the suspension buffer for 200 nm beads. Next, Equation 7 was applied to predict mAb filtration profiles. The rank order of filterability could be predicted using Equation 7, however there were offset in the x axis values when comparing Supporting Information S1: Figure S1a with Figure S9. Therefore, a correction factor, α , was employed as described in Table 2a. Figure 4 shows curve fitting results for Equation 7 that contain α . Further fitting results are shown in Supporting

Information S1: Figure S10. To offset the x axis, an appropriate α value is required. Better fitting results could be obtained when α is introduced only to 200 nm particles, compared to the case when introducing α to all particle sizes. It is considered that intermediate blocking for 200 nm particles was occurred at the secondary layer of Filter A. It is suggested that α offsets the interactions between protein aggregates and filter matrix, and inter-protein aggregates. A linear relationship between the concentration of 200 nm particles and the α value is shown in Figure 5a,

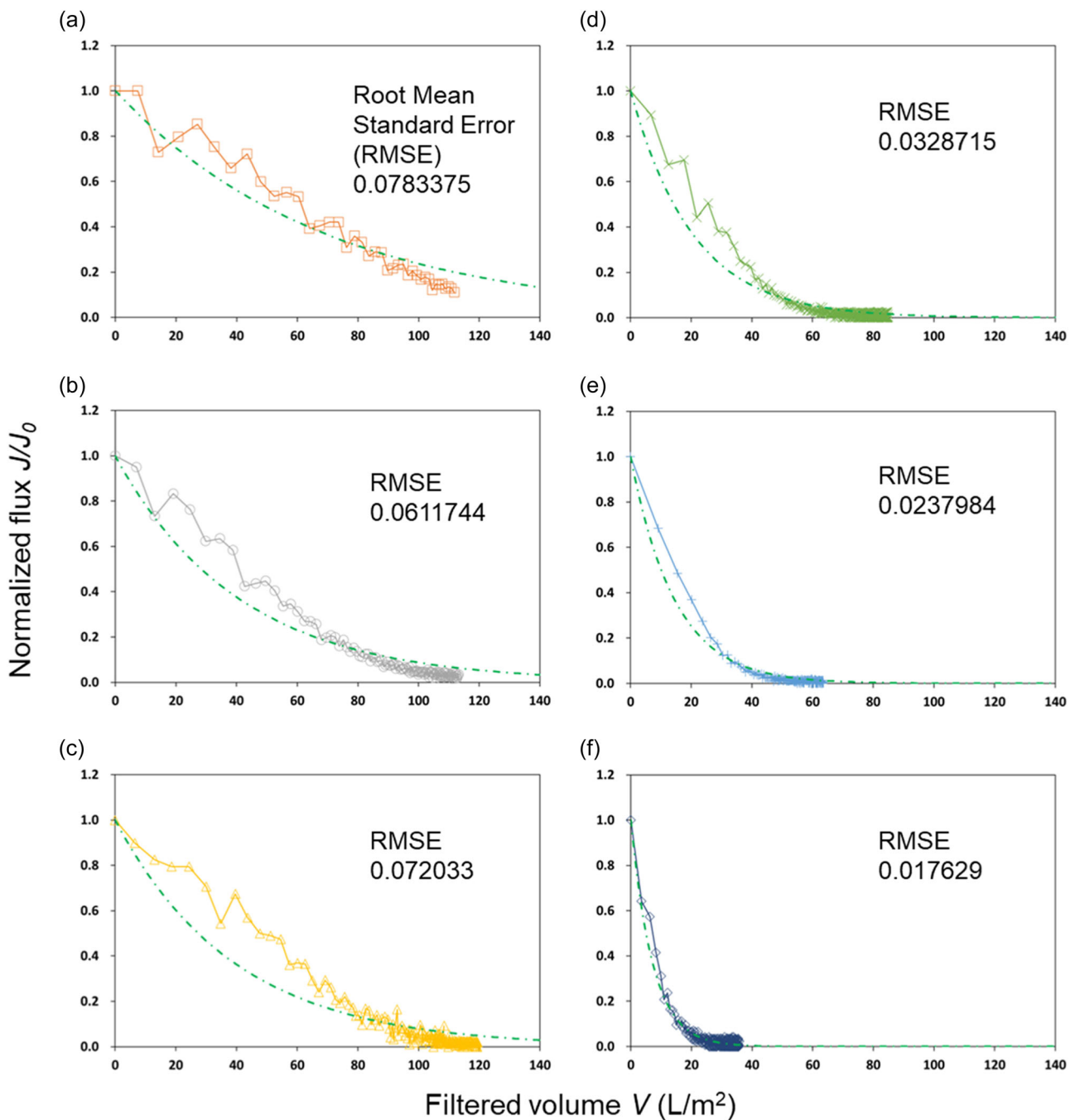


FIGURE 4 Predicted filtration profiles for six monoclonal antibodies with Filter A. Experimental results were plotted and dashed lines represent predicted filtration profiles. Samples: (a–f) mAb1–6, respectively.

and α was in inverse proportion to the concentration of 200 nm particles as shown in Figure 5b. Experimental versus predicted results of V_{\max} including seven mAbs (mAb1–7) and an Fc-fusion protein (Fc-fusion1) are plotted in Figure 6a; here the predicted results showed good agreement with the experimental results. Thus, this prediction model could be applied to various therapeutic proteins not only mAbs but also Fc-fusion proteins in buffers which have wider range of conductivity. The experimental results of V_{\max} were calculated as described in the Materials and Methods section, while the predicted results of V_{\max} were

determined by the volume (V) and the value predicted by Equation 7 when $J/J_0 = 0.05$. Both these V_{\max} values were consistent (Figure 6a).

Using the same approach, we developed a prediction model for the flux decay profile for filter B which has different membrane material and internal structure with filter A. Filtration results for the model beads are shown in Supporting Information S1: Figures S11 and S12. Particles $\leq 2 \mu\text{m}$ caused filter fouling, while those $\geq 4 \mu\text{m}$ did not cause filter fouling with Filter B. Table 2b shows the details of the model equation for Filter B. The best fit model for filter fouling caused by particles

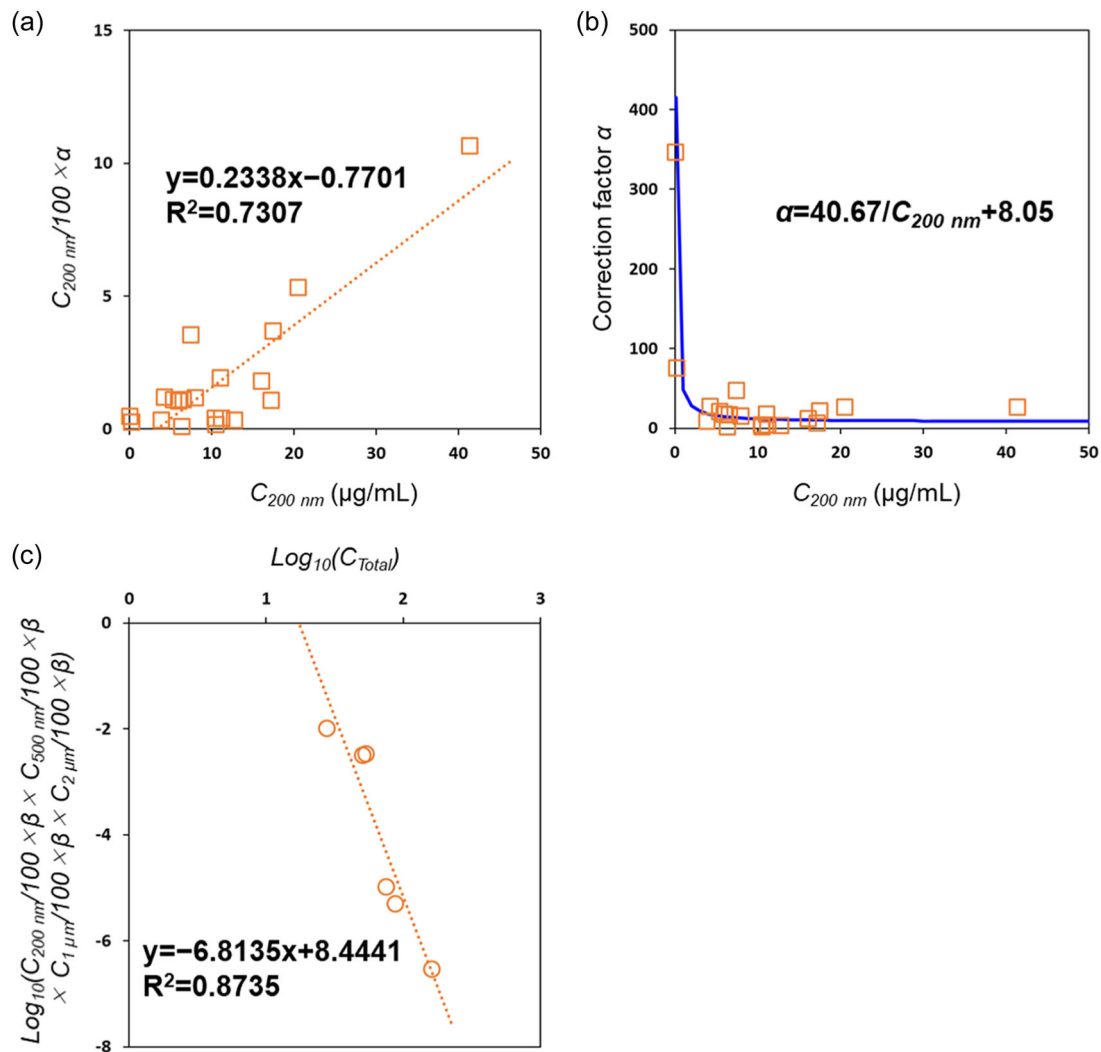


FIGURE 5 Relationship between the particle concentration and correction factors. (a) Relationship between the concentration ($C_{200 \text{ nm}}$) and the correction factor α for the prediction model using Filter A. (b) α is inversely proportional to $C_{200 \text{ nm}}$. (c) Relationship between the concentration of particles (sized 200 nm to 2 μm) and the correction factor β for the prediction model for Filter B. $C_{\text{Total}} = C_{200 \text{ nm}} + C_{500 \text{ nm}} + C_{1 \mu\text{m}} + C_{2 \mu\text{m}}$.

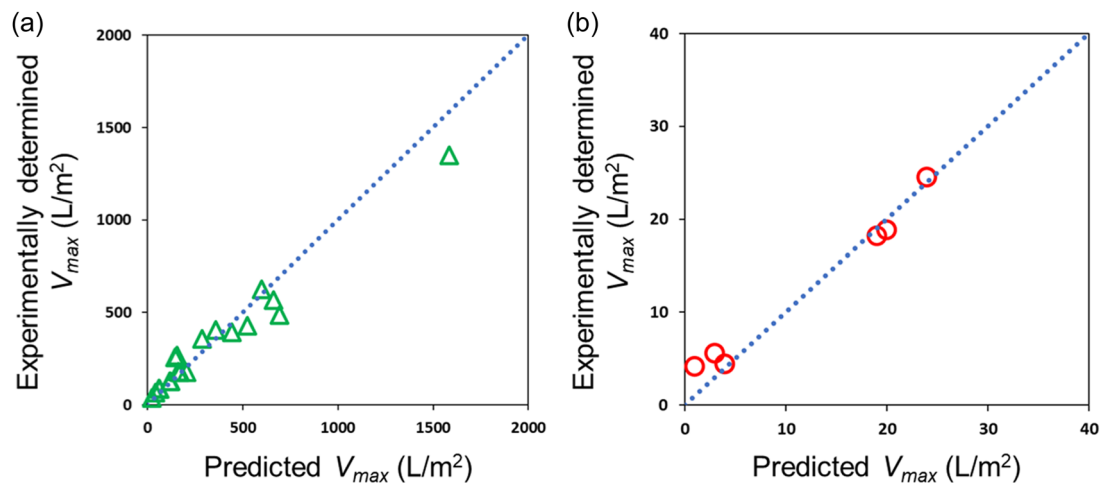


FIGURE 6 Deviations between predicted and experimentally determined V_{max} . (a) Results for Filter A with seven mAbs (mAb1–7) and an Fc-fusion protein (Fc-fusion1). (b) Results for Filter B with six mAbs (mAb1–6).

ranging from 200 nm to 2 μm was the cake filtration model in common. To offset the x axis, the correction factor, β , was introduced to all particle sizes equally. Herewith, the prediction model for flux decay profiles of filter B was successfully established (Figures 5c and 6b, and Supporting Information S1: S13). The correction factor β is considered to offset the density of cake layer. With assumption that hydrodynamic diameters are same, protein aggregates can form much dense cake layer compared with hard-sphere particles like PSL and silica beads. Since the fouling mechanism for 500 nm, 1 μm , and 2 μm are cake filtration, we attempted to introduce β for 500 nm, 1 μm , and 2 μm , and fit the model equation for Filter A to experimental filtration profiles. However, RMSE values were similar to the case when introducing α only to 200 nm. It is thus suggested that 200 nm particles have larger contribution to Filter A fouling compared with other particle sizes. We considered that this model construction approach can be applied to protein low-adsorption MF filters which is generally used for the filtration of protein solutions. If the case that the membrane has surface modifications, further

improvements considering protein-substrate interactions may be necessary.

3.5 | Initial flux predictions based on solution viscosity

We used the Hagen-Poiseuille equation to develop a prediction method for initial flux; this is shown as Equation 8:

$$Q = \pi r^4 \Delta p / 8 \mu L. \quad (8)$$

Here Q is the volumetric flow rate, r is the cylindrical pipe radius, Δp is the pressure difference between the two ends of the pipe, μ is the viscosity, and L is the length of the pipe. This equation is also the basis of filter fouling models mentioned in the previous section (i.e., Equations 2-6). Equation 8 can be transformed to Equation 9.

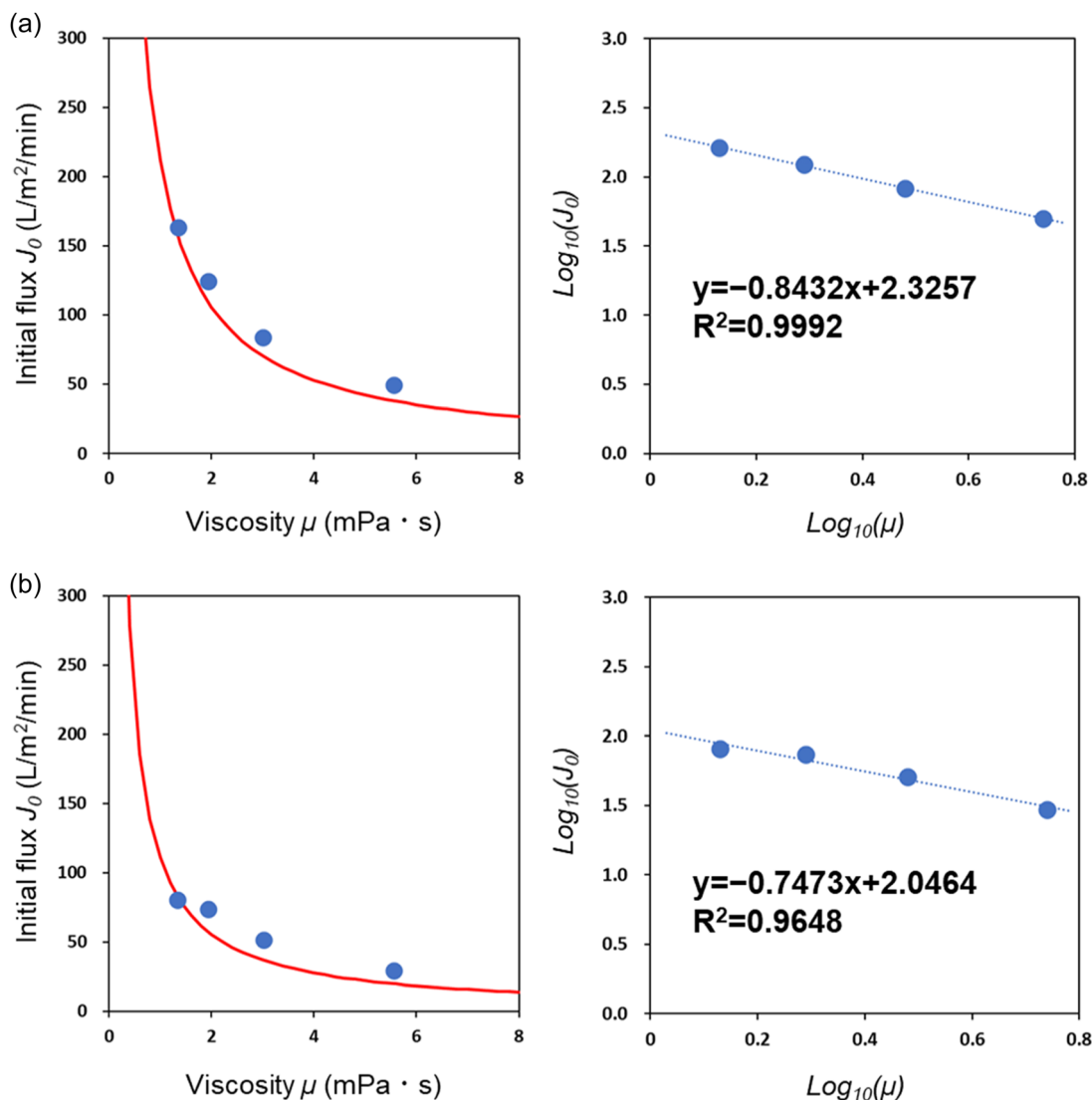


FIGURE 7 Calibration curve determining initial flux by the viscosity based on the Hagen-Poiseuille equation using Filters (a) A and (b) B.

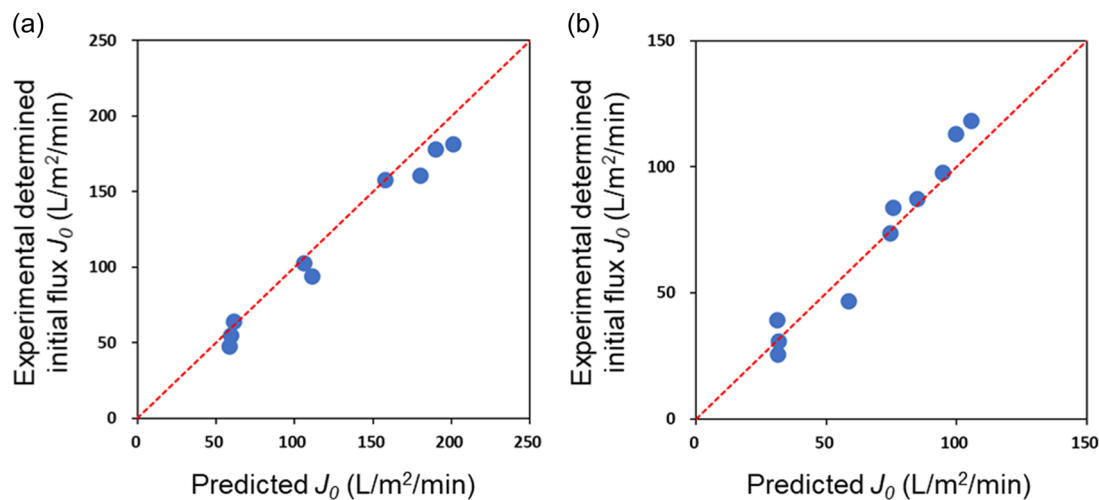


FIGURE 8 Deviations between the predicted initial flux J_0 and the experimentally determined J_0 for several mAb8 samples and three buffers using Filters (a) A and (b) B.

$$Q \times \mu = \pi r^4 \Delta p / 8L \quad (9)$$

Here, the MF filter is assumed to be a cylindrical pipe with a radius and length of r and L , respectively. When the filtration experiment is conducted under constant pressure conditions, Δp can be considered as a constant. Based on these parameters, the right side of Equation 9 can be regarded as the constant value for each MF filter. Therefore, the initial flux can be predicted from the solution viscosity. Figure 7 shows the relationship between the viscosity and the initial flux for trehalose solutions with both Filters A and B. The Hagen–Poiseuille equation fits these data well. Using the fitting curves indicated in Figure 7, the initial flux was predicted for several mAb8 samples and three buffers—that is, 10 mM histidine with 5% sorbitol (pH 5.5), 120 mM acetate buffer (pH 5.0), and 50 mM acetate buffer (pH 5.0) with 0.2 M NaCl. Prediction results for Filters A and B shown in Figure 8 indicate that the initial flux predictions were successful for both Filters A and B. By combining two prediction models—that is, for the flux decay profile and the initial flux—it is then possible to predict the entire MF profile.

4 | CONCLUSION

We successfully established a prediction model for the flux decay profiles of biopharmaceuticals using two different MF filters which have different membrane materials and internal structures. In addition, the initial flux could predict using the Hagen–Poiseuille equation for both filters. Our findings suggest that this approach can be applied to various MF filters for proteins. These models facilitate effective MF scale-up assessment during the early stages of process development. By evaluating the characteristics of each filter using model beads, the filterability of each MF filter will be able to simulate and compared by their protein aggregate profiles. Obtaining quantitative data for protein aggregates under different process parameters can then help to evaluate how these parameters affect

aggregate formation and MF filterability. Moreover, this methodology can be applied for assessing the manufacturability of biopharmaceutical candidates based on the propensity for subvisible particle formation and the solution viscosity.

ACKNOWLEDGMENTS

This study was partially supported by a grant from Japan Agency for Medical Research and Development (AMED) [22ae0121013h0602 and 22ak0101188j0001 to Susumu Uchiyama].

CONFLICT OF INTEREST STATEMENT

Kota Inoue, Yumiko Masuda, and Koichi Nonaka are employees of Daiichi Sankyo Co., Ltd.

DATA AVAILABILITY STATEMENT

The data that support the findings of this study are available from the corresponding author upon reasonable request.

ORCID

Kota Inoue  <https://orcid.org/0009-0001-8709-8682>

Yumiko Masuda  <https://orcid.org/0000-0001-5548-7520>

Tetsuo Torisu  <http://orcid.org/0000-0002-8269-7803>

Koichi Nonaka  <https://orcid.org/0000-0002-2643-4718>

Susumu Uchiyama  <http://orcid.org/0000-0002-5181-179X>

REFERENCES

- Bolton, G. R., Boesch, A. W., & Lazzara, M. J. (2006). The effects of flow rate on membrane capacity: Development and application of adsorptive membrane fouling models. *Journal of Membrane Science*, 279(1–2), 625–634. <https://doi.org/10.1016/j.memsci.2005.12.057>
- Breite, D., Went, M., Prager, A., Kuehnert, M., & Schulze, A. (2019). Charge separating microfiltration membrane with pH-dependent selectivity. *Polymers*, 11(1), 3. <https://doi.org/10.3390/polym11010003>
- Callahan, D. J., Stanley, B., & Li, Y. (2014). Control of protein particle formation during ultrafiltration/diafiltration through interfacial

- protection. *Journal of Pharmaceutical Sciences*, 103(3), 862–869. <https://doi.org/10.1002/jps.23861>
- Gikanga, B., Chen, Y., Stauch, O. B., & Maa, Y. F. (2015). Mixing monoclonal antibody formulations using bottom-mounted mixers: Impact of mechanism and design on drug product quality. *PDA Journal of Pharmaceutical Science and Technology*, 69(2), 284–296. <https://doi.org/10.5731/pdajpst.2015.01031>
- Gikanga, B., Eisner, D. R., Ovadia, R., Day, E. S., Stauch, O. B., & Maa, Y. F. (2017). Processing impact on monoclonal antibody drug products: Protein subvisible particulate formation induced by grinding stress. *PDA Journal of Pharmaceutical Science and Technology*, 71(3), 172–188. <https://doi.org/10.5731/pdajpst.2016.006726>
- Gikanga, B., & Maa, Y. F. (2020). A review on mixing-induced protein particle formation: The puzzle of bottom-mounted mixers. *Journal of Pharmaceutical Sciences*, 109(8), 2363–2374. <https://doi.org/10.1016/j.xphs.2020.03.024>
- Han, Q., Li, W., Trinh, T. A., Fane, A. G., & Chew, J. W. (2018). Effect of the surface charge of monodisperse particulate foulants on cake formation. *Journal of Membrane Science*, 548, 108–116. <https://doi.org/10.1016/j.memsci.2017.11.017>
- Her, C., & Carpenter, J. F. (2020). Effects of tubing type, formulation, and postpumping agitation on nanoparticle and microparticle formation in intravenous immunoglobulin solutions processed with a peristaltic filling pump. *Journal of Pharmaceutical Sciences*, 109(1), 739–749. <https://doi.org/10.1016/j.xphs.2019.05.013>
- Ishikawa, T., Kobayashi, N., Osawa, C., Sawa, E., & Wakamatsu, K. (2010). Prevention of stirring-induced microparticle formation in monoclonal antibody solutions. *Biological and Pharmaceutical Bulletin*, 33(6), 1043–1046. <https://doi.org/10.1248/bpb.33.1043>
- Joseph, A., Kenty, B., Mollet, M., Hwang, K., Rose, S., Goldrick, S., Bender, J., Farid, S. S., & Titchener-Hooker, N. (2016). A scale-down mimic for mapping the process performance of centrifugation, depth and sterile filtration. *Biotechnology and Bioengineering*, 113(9), 1934–1941. <https://doi.org/10.1002/bit.25967>
- Minow, B., Rogge, P., & Thompson, K. (2012). Implementing a fully disposable mAb manufacturing facility. *BioProcess International*, 10(6), 48–57.
- Nayak, A., Colandene, J., Bradford, V., & Perkins, M. (2011). Characterization of subvisible particle formation during the filling pump operation of a monoclonal antibody solution. *Journal of Pharmaceutical Sciences*, 100(10), 4198–4204. <https://doi.org/10.1002/jps.22676>
- Nikfarjam, L., & Farzaneh, P. (2012). Prevention and detection of Mycoplasma contamination in cell culture. *Cell Journal*, 13(4), 203–212.
- Robertson, J. H., Wilson, J. D., Bing, F., Byrd, M., Feeser, T. M., Jornitz, M. W., Levy, R. V., Madsen, R. E., Martin, J. M., Meissner, L. S., Meltzer, T. H., Morris, G. M., Nordhauser, F. M., Pietro, J., Schroeder, H. G., Stinavage, P. S., Trotter, A. M., Waibel, P. J., Weber, B. L., ... Wolber, P. (1998). Sterilizing filtration of liquids. Technical report no. 26. *PDA Journal of Pharmaceutical Science and Technology*, 52(Suppl. 1), 1–31.
- Seddiq, A. S., van Duijvenvoorde, R. B., Jiskoot, W., & Nejadnik, M. R. (2016). No touching! Abrasion of adsorbed protein is the root cause of subvisible particle formation during stirring. *Journal of Pharmaceutical Sciences*, 105(2), 519–529. <https://doi.org/10.1016/j.xphs.2015.10.003>
- Solomon, D. E., Abdel-Raziq, A., & Vanapalli, S. A. (2016). A stress-controlled microfluidic shear viscometer based on smartphone imaging. *Rheologica Acta*, 55(9), 727–738. <https://doi.org/10.1007/s00397-016-0940-9>
- Totoki, S., Yamamoto, G., Tsumoto, K., Uchiyama, S., & Fukui, K. (2015). Quantitative laser diffraction method for the assessment of protein subvisible particles. *Journal of Pharmaceutical Sciences*, 104(2), 618–626. <https://doi.org/10.1002/jps.24288>
- Trinh, T. A., Li, W., & Chew, J. W. (2020). Internal fouling during microfiltration with foulants of different surface charges. *Journal of Membrane Science*, 602:117983. <https://doi.org/10.1016/j.memsci.2020.117983>
- Tucker, I. M., Corbett, J. C. W., Fatkin, J., Jack, R. O., Kaszuba, M., MacCreath, B., & McNeil-Watson, F. (2015). Laser Doppler electrophoresis applied to colloids and surfaces. *Current Opinion in Colloid & Interface Science*, 20(4), 215–226. <https://doi.org/10.1016/j.cocis.2015.07.001>
- Wu, H., & Randolph, T. W. (2020). Aggregation and particle formation during pumping of an antibody formulation are controlled by electrostatic interactions between pump surfaces and protein molecules. *Journal of Pharmaceutical Sciences*, 109(4), 1473–1482. <https://doi.org/10.1016/j.xphs.2020.01.023>
- Yoneda, S., Niederleitner, B., Wiggernhorn, M., Koga, H., Totoki, S., Krayukhina, E., Friess, W., & Uchiyama, S. (2019). Quantitative laser diffraction for quantification of protein aggregates: Comparison with resonant mass measurement, nanoparticle tracking analysis, flow imaging, and light obscuration. *Journal of Pharmaceutical Sciences*, 108(1), 755–762. <https://doi.org/10.1016/j.xphs.2018.09.004>
- Zydney, A. L., & Ho, C. C. (2002). Scale-up of microfiltration systems: Fouling phenomena and Vmax analysis. *Desalination*, 146(1–3), 75–81. [https://doi.org/10.1016/S0011-9164\(02\)00492-7](https://doi.org/10.1016/S0011-9164(02)00492-7)

SUPPORTING INFORMATION

Additional supporting information can be found online in the Supporting Information section at the end of this article.

How to cite this article: Inoue, K., Masuda, Y., Torisu, T., Nonaka, K., & Uchiyama, S. (2024). Prediction models for the flux decay profile and initial flux of microfiltration for therapeutic proteins. *Biotechnology and Bioengineering*, 1–13. <https://doi.org/10.1002/bit.28692>